

Study of snow water equivalence inversion technique with simulating model

Lingmei Jiang^{a,b}, J Shi^a, Saibun Tjuatja^c, K.S Chen^d

^aInstitute for Computational Earth System Science, University of California, Santa Barbara, U.S.A;

^bResearch Center for Remote Sensing and GIS, School of Geography, Beijing Normal University, China;

^cDepartment of Electrical Engineering, the University of Texas at Arlington, U.S.A;

^dCenter for Space and Remote Sensing Research, National Central University, Chung-Li, 32054

ABSTRACT

In this paper, we evaluate the capability of a multi-scattering microwave emission model that including the Dense Media Radiative Transfer Model (DMRT) and AIEM to simulation of dry snow emission with Matrix Doubling approach. We compared the predictions of this model with the ground experimental measurements. The comparison showed that our snow microwave emission model agreed well with the experimental measurements. In order to develop retrieval snow properties: snow depth or snow water equivalence (SWE) retrieval algorithm, we carried out the sensitivity test between the emission models with the different scattering-order: the zeroth-order, the first-order and the multi-scattering models. The results indicated that the multi-scattering effects have to be taken into account in the snow emission model, especially for large grain size. Due to the complexity of the multi-scattering model, we developed a parameterized inversion model using our multi-scattering emission model with a wide range of snow and under-ground properties for algorithm development purpose.

Keywords- snow, passive microwave remote sensing, parameterization

1. INTRODUCTION

Snow water equivalence (SWE), the product of density and depth, is often the variable of most interest to hydrologists because it represents the amount of water potentially available for runoff. Measurement of the amount of water stored in the snowpack and forecasting the rate of melt are thus essential for management of water supply. Because microwave radiation penetrates through snow, microwave remote sensing retrieval of snow parameters, such as snow extent, snow water equivalent, and wet/dry state, have been investigated by many researchers using various microwave sensors with various degree of success^{1,2,3,4,5}. At coarse resolution, for global and continental scale, snow has been a focus of passive microwave remote sensing since its inception. Passive microwave remote sensing can provide useful information at large scale on snow cover characteristics for hydrological, climatic, and meteorological applications.

Microwave brightness temperature measurements between 3 GHz and 90 GHz have found sensitive to snow type and water equivalent⁶. At the lower frequencies of the microwave band, emission from a dry snow cover is mainly affected by underlying soil dielectric and roughness properties. At the higher frequencies, however, emission is sensitive to snow water equivalence and snow particle size since the volume scattering by snow particles becomes important^{7,8}. Because dry snow emits considerably less microwave radiation than soil, the brightness temperature of snow is inversely related to the snow-water equivalence, and the measurements can be carried out through cloud cover. When snow starts to melt, emission will significantly increase due to the high dielectric contrast between ice and liquid water in microwave spectrum and the observed signals are only emitted from the near snow surface⁹.

For this paper, we describe our snow emission model in next section. The comparisons of our microwave emission model with the ground experimental measurements from¹⁰ are demonstrated in section 3. The sensitivity test for the snow emission models with the different scattering order is discussed in section 4. In the last section, we show a parameterized snow emission model for snow inversion model development.

2. MODEL DESCRIPTION

The radiative transfer model can be solved exactly by numerical methods, such as Matrix Doubling method¹¹ or the eigen-analysis technique^{11,12}. For our snow emission model (see Figure 1), the Matrix Doubling approach is used

to solve the vector radiative transfer equations to include the multi-scattering effects. This model uses 1) the dense media model (DMRT) with the Mie scattering assumption¹³ to describe snow pack extinction and emission properties and 2) the Advanced Integral Equation Model (AIEM)¹⁴ to calculate the subsurface emission signal, and to calculate the boundary conditions at the snow-air and snow-soil interfaces for the vector radiative transfer model.

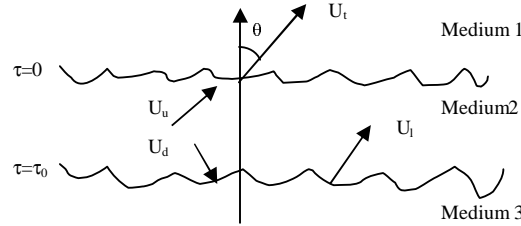


Fig.1 Geometry of the single layer emission problem.

2.1 The Matrix Doubling method

The Matrix Doubling method which considers multi-scattering effects is a numerical solution to radiative transfer equations. There were three major emission sources for an inhomogeneous layer: upwelling and downwelling of emitted intensities within the snow layer; upward emission from the lower half space. These intensities were expected to go through some or all of the following processes, volume scattering, surface scattering, attenuation, surface-volume interactions and transmission across irregular boundary or boundaries, before they arrive at the receiver.

The total emission u_t into the medium due to u_u , u_d and u_1 may be written

$$u_t = L_u u_u + L_d u_d + L_1 u_1 \quad (1)$$

where L 's are the multiple scattering operators.

u_u : the total upward emission from the layer.

u_d : the total downward emission from the layer.

u_1 : the emission from the lower homogeneous half space.

The matrix-doubling method provides an alternative to the radiative transfer method for computing the combined scattering effects of surface and volume scattering. It is also based on energy balance and has been shown to be an equivalent formulation to the radiative transfer approach¹⁵. In actual computation this is a more efficient method for layers having large optical thickness, but it is not suitable for extension to multilayered media.

2.2 The Advanced Integral Equation Method (AIEM)

At the interface between two homogeneous media, the scattering characteristics are determined by the interface roughness and the discontinuity between the media. Several surface scattering models have been developed in the last three decades¹⁶. They are the small perturbation model (SPM), Kirchhoff model (KM), phase perturbation model (PPM), full wave model (FWM), and the integral equation model (IEM)¹⁷. The IEM was verified by laboratory measurements of bistatic scattering from surfaces with small, intermediate and large scale roughness. And the advanced IEM (AIEM) kept the absolute phase term in Greens function, meaning which has more accuracy than the old IEM¹⁴. So we applied AIEM to deal with boundary effects in this study.

The bistatic scattering coefficient can be expressed

$$\sigma_{qp}^s = \sigma_{qp}^k + \sigma_{qp}^{kc} + \sigma_{qp}^c = \frac{k_1^2}{2} \exp \left[-\sigma^2 (k_z^2 + k_{sz}^2) \right] \sum_{n=1}^{\infty} \sigma^{2n} \left| I_{qp}^n \right|^2 \frac{W^{(n)}(k_{sx} - k_x, k_{sy} - k_y)}{n!} \quad (2)$$

where

$$\begin{aligned}
I_{qp}^n = & (k_{sz} + k_z)^n f_{qp} e^{-\sigma^2 k_z k_{sz}} \\
& + \frac{1}{4} \left\{ (k_{sz} - q_1)^n F_{qp1}^{(+)} e^{-\sigma^2 (q_1^2 - q_1 k_{sz} + q_1 k_z)} \right. \\
& + (k_{sz} - q_2)^n F_{qp2}^{(+)} e^{-\sigma^2 (q_2^2 - q_2 k_{sz} + q_2 k_z)} \\
& + (k_{sz} + q_1)^n F_{qp1}^{(-)} e^{-\sigma^2 (q_1^2 + q_1 k_{sz} - q_1 k_z)} \\
& + (k_{sz} + q_2)^n F_{qp2}^{(-)} e^{-\sigma^2 (q_2^2 + q_2 k_{sz} - q_2 k_z)} \\
& \left. + (k_{sz} + q_2)^n F_{qp2}^{(-)} e^{-\sigma^2 (q_2^2 + q_2 k_{sz} - q_2 k_z)} \right\} \Big|_{u,v=-k_x,-k_y} \\
& + \frac{1}{4} \left\{ (k_{sz} + q_1)^n F_{qp1}^{(+)} e^{-\sigma^2 (q_1^2 - q_1 k_{sz} + q_1 k_z)} \right. \\
& + (k_{sz} + q_2)^n F_{qp2}^{(+)} e^{-\sigma^2 (q_2^2 - q_2 k_{sz} + q_2 k_z)} \\
& + (k_{sz} - q_1)^n F_{qp1}^{(-)} e^{-\sigma^2 (q_1^2 + q_1 k_{sz} - q_1 k_z)} \\
& + (k_{sz} - q_2)^n F_{qp2}^{(-)} e^{-\sigma^2 (q_2^2 + q_2 k_{sz} - q_2 k_z)} \\
& \left. + (k_{sz} + q_2)^n F_{qp2}^{(-)} e^{-\sigma^2 (q_2^2 + q_2 k_{sz} - q_2 k_z)} \right\} \Big|_{u,v=-k_{sx},-k_{sy}}
\end{aligned} \tag{3}$$

where $W^{(n)}(\bullet)$ is the Fourier transform of the n th power of the normalized surface correlation function. The above expression is suitable for small to large $k\sigma$ calculations. When $k\sigma$ is large, only the first term in eq. (4) can be kept in the formulation, which is the Kirchhoff term.

3. COMPARISONS WITH THE EXPERIMENTAL DATA

3.1 The experimental data description

The radiometric measurements that we used for evaluation of our microwave model were from¹⁰. The ground data include temperature, permittivity, density and wetness profiles. The radiometric measurements were obtained with a set of five portable linearly polarized Dicke radiometers that operating at frequencies of 11, 21, 35, 48 and 94 GHz. The radiometers were fixed on a special sledge about 160 cm above ground. The incidence angle varies from 20° to 70°. These passive microwave measurements were complemented by ground observations and radar measurements. In this study, we used the measurements on Dec. 21, 1995 at Weissfluhjoch (46°49, 83'N, 9°48, 62'E) in Davos, Switzerland. These measurements were with four frequencies at both v- and h- polarizations, 11GHz, 21 GHz, 35GHz, 94GHz.

TABLE I. SNOW PROFILE DATA FROM 21 DECEMBER 1995

Layer#	Tsnow(K)	W (%)	ρ (kg/m ³)	d (cm)
1	273.0	0.0	259.0	25.0
2	272.0	0.0	177.0	15.0
3	271.8	0.0	400.0	0.3
4	271.4	0.0	70.0	20.0

* T_{snow} is the snow temperature, W is the liquid water content, ρ the snow density, d the layer thickness. The layer number increases with height above ground

The snow profile data from¹⁵ is shown in Table 1. It is a winter snow situation with a snow height of 60.3 cm. The top layer was 20 cm of new snow, below was a thin crust, and the bottom layer consisted of coarse-grained snow. Then we applied the following input parameters of the model:

- Density of snow: 0.22 g/cm³
- Radius: 0.48 mm
- Snow depth: 0.603m
- Snow temperature: 272.2 K
- Soil surface rms height and correlation length: 1, 20cm
- Soil moisture: 10%

The brightness temperature observed by radiometer (T_b) can be approximated described by the following expression:

$$T_b = T_s + (1-e) \cdot T_{sky} \quad (5)$$

where T_s, e are the emission and emissivity from snowpack and the underlying ground. T_{sky} is the downwelling atmospheric radiation. In this experiment, the sky brightness temperature is observed at 120° incidence angle for the used frequencies. T_{sky} observed in that measurement at 11, 21, 35 and 94 GHz are as 12.8, 41.2, 50.2 and 114 K.

3.2 The comparison results

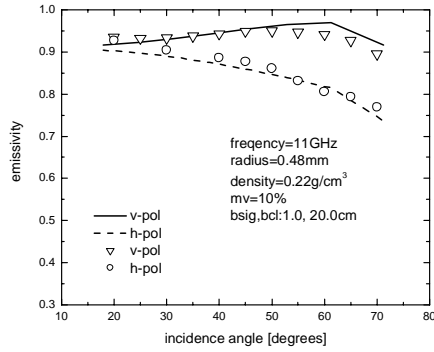


Fig2. Emissivity versus incidence angle at f=11GHz

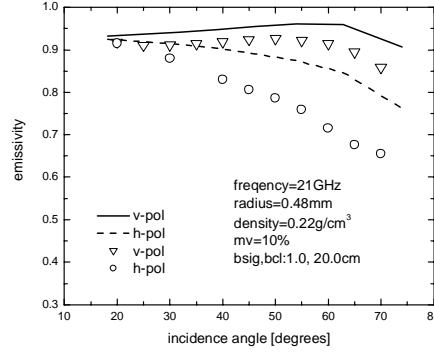


Fig3. Emissivity versus incidence angle at f=21GHz

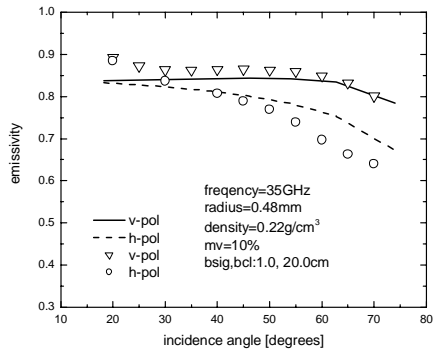


Fig4. Emissivity versus incidence angle at f=35GHz

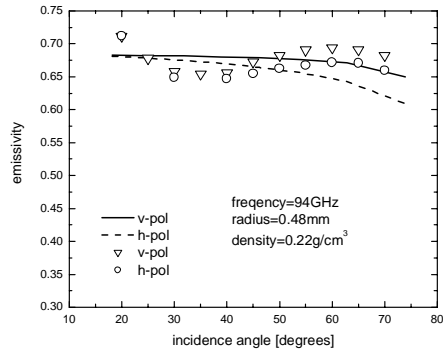


Fig5. Emissivity versus incidence angle at f=94GHz

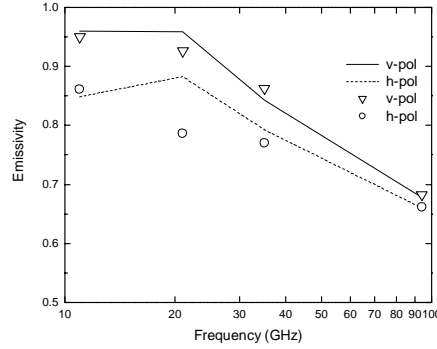


Fig6. Emissivity versus frequency at $\theta = 50^\circ$. Measured (circles and triangles) and simulated (curves) data of the snowpack on 21 Dec. 1995

Figure 2, 3, 4, and 5 indicate the relationship of emissivity with incidence angle at 11 GHz, 21 GHz, 35 GHz and 94 GHz. Figure 6 is that emissivity varies with all the frequencies at 50° incidence angle.

From snow properties given in Table 1, we know the ground surface dielectric and roughness properties couldn't affect on the simulation at 94 GHz. It was found that the simulated emissivity at 94 GHz is very sensitive to snow density. Only a slight change in snow density will result in a significant change in the simulated emissivity. On the other hand, the ground surface dielectric and roughness properties have a great impact on the subsurface emission signals that may dominant at 11 GHz. At 11, 35, 94 GHz, our microwave emission model predictions agree well with the measured data in terms of both magnitudes for v and h-polarizations and their difference. It can be observed that as the frequency increases, the snow emissivity decreases and the difference between v and h polarizations also decreases. Or the emission signals between v and h polarizations become much closer as frequency increases.

At 21 GHz, the model simulated values are obviously higher than the measured data nearly for all incidence angles. It might result from the uncertainties in the experiment data and atmospheric effects at 21 GHz. The contribution from multiple scattering is expected to slow down the angular trend of horizontal emission but not vertical polarization¹⁶. From the measurements, the polarization difference with angular variation has the maximum at 21 GHz. The vertical emissivity at 21 GHz is higher than that at 11 GHz, while the horizontal emissivity is close to that at 35 GHz after 40° incidence angle. Such a result is not in agreement with intuition and our understanding. In addition, we can see the polarization difference at large incident angle decreased with the frequency increasing from 11 GHz to 94 GHz based on the model calculation value.

4. SENSITIVITY TEST ON EFFECTS OF SCATTERING ORDER

For inversion algorithm development of snow depth (SWE) retrieval, we evaluated the effects of multi-scattering on snow emissivity simulation by comparison the multi-scattering model (described in section 2) with the zeroth-order and first-order emission models. The task is to examine the applicability of the simple models (the zeroth and first order scattering) could be used as an inversion model. The zeroth-order and first-order solutions can be solved using iterative techniques. They are easily applied to do inversion due to their simple analytical formulation, and they provide understanding and insight into the physics of the sources and mechanisms of scattering.

4.1 The zeroth-order and first-order solutions

The pair of differential transfer equations for the upward and downward temperature matrices denoted by T^+ , T^- as follows:

$$\frac{d}{dz}T^+(z) = -k_{es}T^+(z) + F^+(z) + k_{as}T \quad (4)$$

$$\frac{d}{dz}T^-(z) = k_{es}T^-(z) - F^-(z) - k_{as}T \quad (5)$$

where $k_{es} = k_e / \cos \theta_s$; $k_{as} = k_a / \cos \theta_s$, $\mu_s = \cos \theta_s$, $T^+(z) = T(z, \mu_s, \phi_s)$, $T^-(z) = T(z, -\mu_s, \phi_s)$. And T is the temperature profile in the layer assumed to be independent of the azimuthal angle.

$$\begin{aligned}
F^\pm(z) &= \frac{k_{ss}}{4\pi} \int_0^{2\pi} \int_0^1 P(\pm\mu_s, \mu, \phi_s - \phi) T^\pm d\mu d\phi \\
&\quad + \frac{k_{ss}}{4\pi} \int_0^{2\pi} \int_0^1 P(\pm\mu_s, -\mu, \phi_s - \phi) T^\mp d\mu d\phi \\
&= \frac{k_{ss}}{2} \int_0^1 P_0(\pm\mu_s, \mu) T^\pm d\mu + \frac{k_{ss}}{2} \int_0^1 P_0(\pm\mu_s, -\mu) T^\mp d\mu
\end{aligned} \tag{6}$$

Here F^\pm is the scattering source function. k_s, k_e are the volume scattering and extinction coefficient matrices taken to be diagonal^{18,19}, $k_{ss} = k_s / \cos\theta_s$ and $P_0(\mu_s, \mu)$ is the zeroth-order Fourier component of the scattering phase matrix. When convert the above differential equations into integral equations yielding

$$T^+(z) = T^+(-d)e^{-k_{es}(z+d)} + \int_{-d}^z [F^+(z') + k_{as}T^+] e^{-k_{es}(z-z')} dz' \tag{7}$$

$$T^-(z) = T^-(0)e^{k_{es}z} + \int_z^0 [F^-(z') + k_{as}T^-] e^{k_{es}(z-z')} dz' \tag{8}$$

The zeroth-order equations are defined by neglecting terms in (4) and (5) or (7) and (8) when k_s is very small, i.e., neglecting the term $F^\pm(z)$, which multiplied by k_s . Then we have the following integral equations for zeroth-order:

$$T_0^+(z) = e^{-k_{es}(z+d)} \left[\frac{1}{2} \Gamma_{12}(\mu_i, \mu_j) T_0^-(-d, \mu_j) + e_g T_g \right] + T_s^+(z, \mu_i) \tag{9}$$

$$T_0^-(z) = e^{k_{es}z} \left[\frac{1}{2} \Gamma_{10}(\mu_i, \mu_j) T_0^-(0, \mu_j) + e_g T_g \right] + T_s^-(z, \mu_i) \tag{10}$$

Thus, after solving the above equations, the total emission in the medium above the layer as zeroth-order solution can be simplified as,

$$T_p^{t0} = (T_s \cdot E_p^v + T_s \cdot E_p^v (1 - E_p^s) L_p + T_g \cdot E_p^s \cdot L_p) \cdot \psi_p \tag{11}$$

where ψ_p, T_s, T_g are the power transmittivity at air-snow interface, snow temperature and ground temperature.

To seek the iterative first-order solution with the same contribution sources as zeroth-order, equations governing the first-order results are obtained by solving the source functions F^\pm in which T^\pm has been replaced by T_0^\pm . Thus, we can derive the first-order solutions similar to the zeroth-order formulation,

$$T_p^{t1} = (T_s \cdot E_p^v + T_s \cdot E_p^v (1 - E_p^s) L_p + T_g \cdot E_p^s \cdot L_p + E_1) \cdot \psi_p \tag{12}$$

where E_1 is the volume scattering due to the single-scattering within snow pack and between snow pack and underground surface. Assuming a temperature profile of the form $T = t_0 + t_1 z$, then

$$\begin{aligned}
E_1(0, \mu_s) &= \int_{-d}^0 F^+(z') e^{k_{es}z'} dz' \\
&\approx \frac{\bar{a}a}{2} \int_0^1 P_0(\mu_s, \mu) \left[C_0 t_0 + \left(\frac{eT_g}{\bar{a}} - t_0 \right) C_1 e^{k_e d/\mu} \right] d\mu \\
&\quad + \frac{\bar{a}a}{2} \int_0^1 P_0(\mu_s, \mu) t_1 \left\{ [(\mu + k_e d) C_1 e^{-k_e d/\mu} - \mu C_0 + k_e C] / k_e \right\} d\mu \\
&\quad + \frac{\bar{a}a}{2} \int_0^1 P_0(\mu_s, -\mu) t_0 (C_0 - C_2) d\mu \\
&\quad + \frac{\bar{a}a}{2} \int_0^1 P_0(\mu_s, -\mu) t_1 (1/k_e) [\mu C_0 + k_e C - \mu C_2] d\mu
\end{aligned} \tag{13}$$

Where a is the albedo, \bar{a} is equal to $1 - a$.

2.2 The sensitivity test for the three different scattering-order solutions

For comparisons of the different scattering order emission models, we evaluated the effect of snow particle size in terms of the volume scattering albedo on snow emission simulations. This was done by only varying the snow particle sizes with the other fixed snow pack (temperature, density, and depth) and underground (dielectric and roughness) properties. Figure 7 shows the simulated brightness temperature (y-axis) at 18.7 GHz as a function of the volume scattering albedo (x-axis) for the Matrix Doubling (black square), first-order (triangle), and zeroth-order (star) models at 0° and 55° viewing angles.

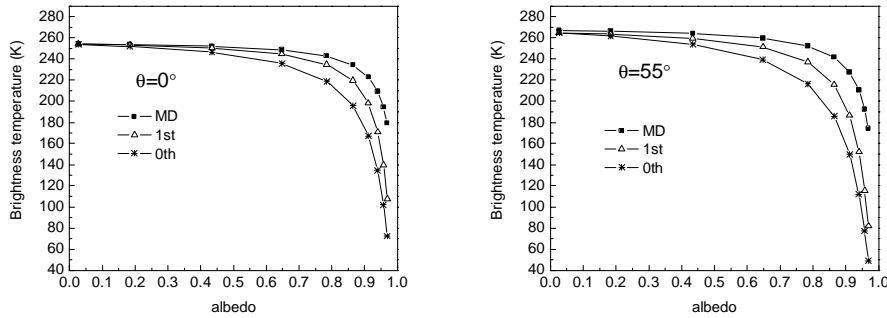


Fig 7. Emission comparison for different scattering-order solutions with different incident angle at V-pol
 *MD – the Matrix Doubling method, 1st – the first-order solutions, 0th – the zeroth-order solutions

Figure 7 shows that when the albedo is small less than 0.2, there are nearly no difference between these three emission models, i.e. the multi-scattering is really very small. For small albedo, we can use zeroth-order or first-order model to simulate snow emission signals. As the volume scattering albedo increases, the differences between these three models became larger and larger due to the multi-scattering effects. We also can see that the emission difference of the scattering-order models at 55° incidence angle is larger than that at 0° incidence angle. Therefore, we must consider the multi-scattering in the microwave snow emission model, especially for the moderate to large grain sizes.

5. A PARAMETERIZED MODEL

In section 3, we demonstrated the microwave emission model considering multi-scattering predicted dry snow emission signal fairly well. And in section 4, we see that the zeroth-order and first-order couldn't predict emission very well with large albedo. Obviously, we couldn't use these simple models as the retrieval algorithm. However, the multi-scattering snow emission model is very complex, no analytic solution, and computational intensive. Therefore, it is necessary to develop a simple parameterized model that can be used as an inversion model. For this purpose, we ranged the outputs of our multi-scattering emission model as a three components model with the direct snowpack emission, underground emission, and their interaction term. This three components model is exactly in form of the zeroth-order model (See Eq. (14)).

$$\begin{cases} E_p^t = (E_p^v + E_p^{vs} + E_p^s \cdot L_p) \cdot \Psi_p \\ E_{mp}^t = (E_{mp}^v + E_{mp}^{vs} + E_p^s \cdot L_p) \cdot \Psi_p \end{cases} \quad (14)$$

where E_p^v , E_p^{vs} and E_p^s are the snowpack, interaction and underground emissivity in the zeroth-order form. While E_{mp}^v , E_{mp}^{vs} , E_p^s are the snowpack, interaction and underground emissivity in the multi scattering order form.

As an example of developing the parameterized model under AMSR-E sensor configurations, we established the simulated database that covers the most possible natural snow and underground properties with our multi-scattering snow emission model at the frequencies of 10.9, 18.7, and 36.5 GHz at 55° incidence angle. The output has three components as indicated in Eq. (15). Through our analyses and comparison with the components of the zeroth-order, we find that the direct snow pack emission component with multi-scattering can be approximated as

$$E_{mp}^v \approx E_p^v \cdot Cf_p^v \quad (15)$$

Where E_p^v is the direct snow volume emission in the zeroth-order form. Cf_p^v is the correction factor that corrects the difference in predication of the direct volume emission signal between the zeroth-order and multi-scattering models. Cf_p^v can be expressed as

$$Cf_p^v = \exp(a + b \cdot \log(L_p) + c \cdot \omega + d \cdot \omega^2 \cdot \log(L_p) + e \cdot \omega^3 \cdot \log(L_p)) \quad (16)$$

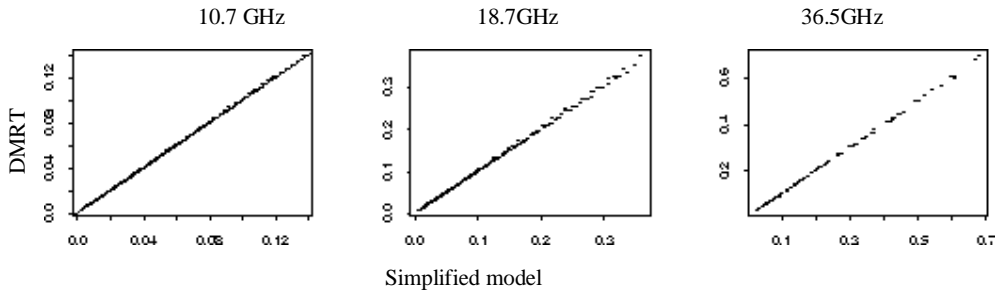


Fig. 8 The comparison between DMRT and simplified model for snowpack emission.

In addition, the sum of interaction and ground emission can be parameterized as

$$E_{mp}^{sv} + E_p^s \cdot L_p \approx E_p^s \cdot Cf_p^{svs} \quad (17)$$

Where the correction factor Cf_p^{svs} can be expressed as

$$Cf_p^{svs} = L_p \cdot \exp(a + b \cdot \log(L_p) + c \cdot \omega + d \cdot \omega \cdot \log(L_p) + e \cdot (\omega \cdot \log(L_p))^2) \quad (18)$$

where ω is albedo, L_p is attenuation factor in the snow pack. The regression coefficients a, b, c, d, e in the eq. (16), (18) are related to frequencies and incidence angles. All the above simplified models agreed well with the theoretical model when snow depth is larger than penetration depth.

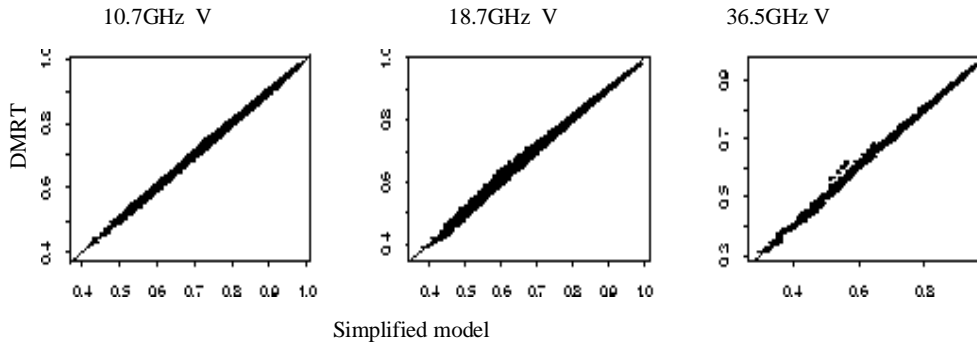


Fig. 10 The comparison between DMRT and simplified model for the sum of interaction term and ground emission at V-pol.

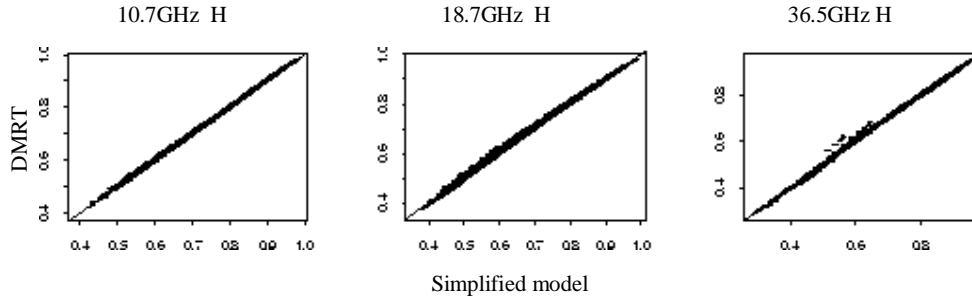


Fig. 11 The comparison between DMRT and simplified model for the sum of interaction term and ground emission at H-pol.

The table2 is the RMSE (Standard error) of simplified model with theoretical DMRT.

Table2. The RMSE of simplified model VS. DMRT

RMSE	10.7 GHz	18.7GHz	36.5GHz
Snowpack emission	0.0004	0.0023	0.004
Sum of interaction term and ground emission (V)	0.004	0.008	0.001
Sum of interaction term and ground emission (H)	0.0084	0.015	0.016

From the above comparison, as can be seen that this parameterized model approach the theoretical model fairly well at 55° incident angle. The RMSE at 10.7 GHz are the smallest both for snow pack and the sum of interaction term and ground emission, because the multi-scattering at lower frequencies is not higher as that at high frequencies. The multi-scattering plays more important role in total snow emission prediction with frequencies increasing. The parameterized model provides us a simple way to simulate snow emission signals and a possibility for snow algorithm development.

6. CONCLUSIONS

This study demonstrates a multi-scattering snow emission model. The experimental data on microwave emission from dry snow collected on Weissfluhjoch has been compared with theoretical simulations performed with our microwave emission model. The results indicate our model predicting dry snow emission signals fairly well. In addition, from the sensitivity test in section 4, it can be seen that we must take into account the multi-scattering in the snow layer emission when snow particle size is from moderate to large. Finally, we develop a parameterized model to simplify the complex but accurate emission model.

ACKNOWLEDGMENTS

This work was supported by the project of the Natural Science Foundation of China (90302008) and the Special Funds for Major State Basic Research Project (G2000077908).

REFERENCES

1. Goodison, B.E, A. Banga, and R.A. Halliday. 1984. Canada-United States Prairie Snow Cover Runoff Study. Canadian Water Resources Journal, Vol. 9, No. 1, pp. 99-107.
2. M. T. Hallikainen and P. Jolma, "Comparison of algorithms for retrieval of snow water equivalent from Nimbus-7 SMMR data in Finland," IEEE Trans. Geosci. Remote Sensing, vol. 30, pp.124-131, 1992.
3. A.T.C. Chang, J.L. Foster and D.K. Hall, "Nimbus-7 derived global snow cover parameters," Annals of Glaciology, vol. 9, pp. 39-44. 1987.
4. J. Aschbacher, "Land surface studies and atmospheric effects by satellite microwave radiometry," Ph. D. dissertation, Univ. of Innsbruck, 1989.

5. J.L. Foster, A.T.C. Chang and D.K. Hall, "Comparison of snow mass estimates from a prototype passive microwave snow algorithm, a revised algorithm and snow depth climatology," *Remote Sens. Environ.*, vol. 62, pp. 132-142, 1997.
6. G. Macelloni, S. Alòscia, and et al, *Microwave Emission From Dry Snow: A Comparison of Experimental and Model Results*, *IEEE Trans. Geosci. Remote Sens.*, Vol. 39, No. 12, pp. 2649-2656, Dec., 2001.
7. R. Hofer and C. Matzler, "Investigation of snow parameters by radiometry in the 3- to 60-mm wavelength region," *J. Geophys. Res.*, vol. 85, pp. 453-460, 1980.
8. H. Rott and K. Sturm, "Microwave signature measurements of Antarctic and Alpine snow," in *Proc. 11th EARSeL Symp.*, Graz, Austria, 1991, pp. 140-151.
9. M. T. Hallikainen, F. T. Ulaby, and T. E. Van Deventer, "Extinction behavior of dry snow in the 18-90 GHz range," *IEEE Trans Geosci. Remote Sensing*, vol. GE-25, pp.737-745, 1987.
10. Wiesmann, A., Stozzi, T., and Weise, T. (1996), *Passive microwave signature catalogue of snowcovers at 11, 21, 35, 48 and 94 GHz*, IAP Research Report 96-8, University of Bern, Switzerland.
11. Ulaby, F. T., R. K. Moore and A. K. Fung, *Microwave Remote Sensing*, Vol. 3, Artech House, Norwood, MA, 1986, Appendix E and Chapter 13.
12. Tsang, L., J. A. Kong and R. T. Shin, *Theory of Microwave Remote Sensing*, John Wiley & Sons, 1985.
13. L. Tsang, "Dense media radiative transfer theory for dense discrete random media with particles of multiple sizes and permittivities," *Prog. Electromag. Res.* 6, vol. 5, pp. 181-225, 1992.
14. K. S. Chen, T. D. Wu, et al., "Emission of rough surfaces calculated by the Integral Equation Method with comparison to three-dimensional moment method simulations", *IEEE trans. Geosci. Remote Sens.*, vol. 41, no. 3, pp. 90-101, 2003.
15. Twomey, S., H. Jacobowitz and H. B. Howell, "Matrix Methods for Multiple-Scattering Problems", *J. Atmos. Sci.*, Vol. 23, pp.289-296, 1966.
16. Ulaby, F.T., R.K. Moore and A. k. Fung, *Microwave remote sensing*, vol.2, Artech House. Norwood, MA, 1982, Chapter 12.
17. A. K. Fung, *Microwave Scattering and Emission Models and Their Applications*. Norwood, MA: Artech House, 1994.